Applied Catalysis B: Environmental 170-171 (2015) 83–89

Contents lists available at ScienceDirect

Applied Catalysis B: Environmental

journal homepage: www.elsevier.com/locate/apcatb

Photocatalytic activity of TiO_2-embedded fluorinated transparent coating for oxidation of hydrosoluble pollutants in turbid suspensions

Federico Persico[a,b], Maurizio Sansotera[a,b,*], Claudia L. Bianchi[b,c], Carlo Cavallotti[a], Walter Navarrini[a,b,*]

[a] Dipartimento di Chimica, Materiali e Ingegneria Chimica "Giulio Natta", Politecnico di Milano, Via Mancinelli 7, 20131 Milano, Italy
[b] Consorzio Interuniversitario Nazionale per la Scienza e Tecnologia dei Materiali, Via G. Giusti 9, 50121 Firenze, Italy
[c] Dipartimento di Chimica, Università degli Studi di Milano, Via Golgi 19, 20133 Milano, Italy

ARTICLE INFO

Article history:
Received 18 November 2014
Received in revised form 20 January 2015
Accepted 23 January 2015
Available online 24 January 2015

Keywords:
Photocatalysis
Water treatment
Turbid solution
Titanium dioxide
Rhodamine B-base
Advanced oxidation processes

ABSTRACT

The photodegradative activity of titanium dioxide immobilized into a multilayered transparent fluoropolymeric matrix was studied. The photoactive coating was developed by applying a TiO_2-containing fluorinated ionomeric dispersion and a perfluorinated amorphous polymer in an appropriate sequence directly on the UV source. The multilayered coating photocatalytic activity toward hydrosoluble organic pollutants was evaluated in clear as well as in highly turbid conditions obtained by dispersing barium sulfate microparticles in the polluted solution. Rhodamine B-base was chosen as reference organic pollutant. The photoabatement rates with TiO_2-embedded fluorinated coating in clear solution and turbid conditions were 0.0923 min^{-1} and 0.0546 min^{-1}, respectively. In both clear and turbid conditions, TiO_2-embedded transparent coating revealed higher photocatalytic activity than merely dispersed TiO_2. This behavior was particularly evident at low pollutant concentrations. In addition, catalyst immobilization prevented TiO_2 separation and catalyst losses, allowing the development of a simple and efficient continuous apparatus.

1. Introduction

Advanced oxidation processes (AOPs) have been widely recognized as performing alternatives to conventional methods for removal of organic pollutants from water and wastewater [1–3]. In particular, semiconducting transition metal oxides revealed remarkable catalytic properties in the presence of UV light, suggesting new promising applications in the field of photocatalysis [4]. Anatase titanium dioxide, TiO_2, has a band gap of 3.2 eV and, whenever its surface is exposed to radiations with wavelengths below 385–410 nm, pairs of holes (h^+, redox potential +2.53 eV vs. the standard hydrogen electrode (SHE)) and electrons (e^-, redox potential −0.52 eV vs. the SHE) are formed. Electron–hole pairs can either recombine or react with adsorbed electron donor or acceptor molecules [5]. In the presence of water and oxygen, hydroxyl radicals $OH^\bullet$ (redox potential $OH^\bullet/H_2O$ = +2.27 eV vs. the SHE) and superoxide ions $O_2^{-\bullet}$ (redox potential $O_2/O_2^{-\bullet}$ = −0.28 eV vs. the SHE) are generated [5]. These radicalic intermediates are strong oxidizing species able to oxidize organic compounds [6,7]. In addition, it has been demonstrated that $Ti^{IV}OH^{\bullet+}$ takes an active part in the mineralization reaction [3,8,9]. Direct oxidation at the hole site is usually favored in case of highly adsorbed substrates, while the degradation of weakly adsorbed pollutants takes place mainly through hydroxyl radical mediated oxidation [10–13]. Hence, the oxidation of organic compounds could be ascribed either to a direct reaction with the photogenerated holes, or to an indirect reaction with hydroxyl radicals or to a combination of the two [14,15].

The use of photocatalytic TiO_2 in suspension or slurry type reactors has been reported to be well performing especially because of the high surface area of the catalyst available for the treatment (average surface area: 95 m^2/g for pure anatase; 55 m^2/g for commercial TiO_2; 75% anatase, 25% rutile; 25 m^2/g for pure rutile) [16–18]. However, the industrial feasibility of such systems is limited due to the low quantum efficiency reported for slurry processes and because a post-treatment catalyst recovery stage is needed

* Corresponding authors at: Dipartimento di Chimica, Materiali e Ingegneria Chimica "Giulio Natta", Politecnico di Milano, Via Mancinelli 7, 20131 Milano, Italy. Tel.: +39 2 2399 3035; fax: +39 2 2399 3180.
E-mail addresses: maurizio.sansotera@polimi.it (M. Sansotera), walter.navarrini@polimi.it (W. Navarrini).

http://dx.doi.org/10.1016/j.apcatb.2015.01.033
0926-3373/

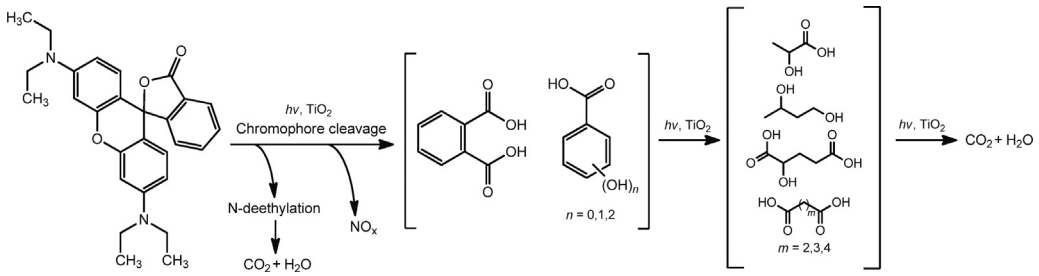

Scheme 1. Photocatalytic degradationof RhB induced by TiO_2.

[5,15]. This additional operation requires a solid-liquid separation stage which adds to the overall cost of the plant [12].

The present work is focused on the development of a perfluorinated multilayered transparent coating with embedded TiO_2 particles able to promote photocatalytic degradation of hydrosoluble organic pollutants, even in turbid solution conditions, and at the same time, overcome the problems related to the post-treatment catalyst recovery stage. An appropriate solid matrix for this application must satisfy several requirements: chemical stability toward UV radiations and UV-activated TiO_2; high transparency toward UV light in order to let UV rays reach the photocatalyst; high permeability to gases, especially to O_2 and water vapor, which are required in the photocatalytic reactions; high wettability in order to optimize the interaction with the polluted aqueous solutions.

The use of perfluoropolymers as coating materials for anodized titanium substrates allows an increase in surface washability, resistance to soiling [14] and gas phase permeability [19,20]. It is well known that soiling on TiO_2 thin layers (e.g., TiO_2 nanotubes by titanium anodizing) can easily deactivate the catalyst [21]. Perfluoropolymeric materials, due to the massive presence of highly stable C—F bonds, as high as 544 kJ/mol [22], are characterized by thermal and chemical stability [22,23], in particular toward UV radiation and UV-activated TiO_2 [24], low surface energy and, if amorphous, also high transparency [14,25]. The interaction between the embedded TiO_2 catalyst and the aqueous polluted solution can be optimized by the use of ionomeric materials. The fluorinated ionomer used in this work is a branched copolymer of tetrafluoroethylene (TFE) and fluorosulfonyl vinyl ether (FSVE) characterized by the presence of strongly acidic groups [26]. Perfluorinated ionomeric membranes have a wide range of applications owing to their excellent chemical and thermal stability, ion conductivity and UV transparency [27,28].

The perfluorinated multilayered ionomeric photoactive coating was directly applied on the quartz sheath of the UV source, allowing the system to treat even turbid solutions. Indeed, the UV-promoted TiO_2 activation and the pollutant diffusion from the aqueous phase to the photoactive coating occurred at the two opposite coating interfaces. The inner interface adherent to the UV source was preserved clean and transparent to UV light; while through the outer interface between the perfluorinated ionomeric coating and the aqueous phase, the pollutants were free to diffuse to the activated TiO_2 nanoparticles dispersed in the ionomeric phase.

The photocatalytic activity of the hybrid coating was evaluated by studying the degradation of Rhodamine B-base (RhB), a hydrosoluble xanthene dye. RhB was chosen as a molecular model of organic pollutant due to its non-biodegradability under aerobic conditions [29,30]. Moreover, aqueous solutions of RhB show a typical red to pink hue due to the strong absorption at 554 nm detectable even at low RhB concentrations (up to 10^{-8} M). This characteristic is not affected by pH variations and allows the monitoring of RhB concentration in solution via spectrophotometric UV–vis analysis [31]. Although the mechanism of photocatalysis has still not been completely clarified, RhB mineralization reaction could be ideally summarized as reported in Eq. (1):

$$C_{28}H_{30}N_2O_3 + (34 + x)O_2 \rightarrow 28CO_2 + 15H_2O + 2NO_x \quad (1)$$

The photocatalytic degradation of RhB in the presence of the photogenerated electron-hole and electron-pairs can be promoted by the direct attack on the central carbon of RhB or by the chromophore cleavage, generating lower MW acids (phthalic, benzoic, hydroxy- and dihydroxy-benzoic); these compounds undergo opening-ring reactions, to give succinic, hydroxypentanedioic, adipic and lactic acids, as well as low MW diols, that are in the end mineralized (Scheme 1) [32,33].

2. Materials and methods

2.1. Materials

Nanometric commercial titanium dioxide P-25 (75% anatase, 25% rutile, Evonik®) in powder was employed as a photocatalyst. As reported in literature, its band gap is between 3.05 and 3.15 eV [34,35]. The photoactive coating applied over the quartz sheath was realized with AQUIVION® D83-06A and HYFLON® AD60 (AQ and AD, respectively – molecular structures in Fig. 1a and b), both produced, commercialized and supplied by Solvay Specialty Polymers. AQ, used as received for the experimental tests, is a melt-extruded ionomeric branched copolymer, obtained from TFE and a Sulfonyl Fluoride Vinyl Ether (SFVE), $F_2C{=}CF{-}O{-}CF_2{-}CF_2{-}SO_2F$. The starting material is in the acidified form, in a 6% solution of 1--propanol (40%), 2-propanol (40%) and water (20%), and it has an equivalent weight of 830 g/eq, total acid capacity of 1.17–1.23 meq/g and density of 0.875 g/cm^3. The SO_3H groups are placed as terminals of the lateral chains, conferring

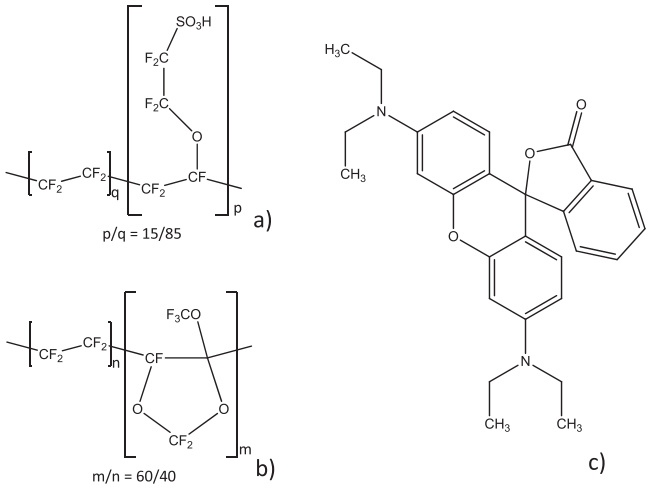

Fig. 1. Molecular structures of Aquivion® D83-06A (a); Hyflon® AD60 (b); and Rhodamine B-base (c).

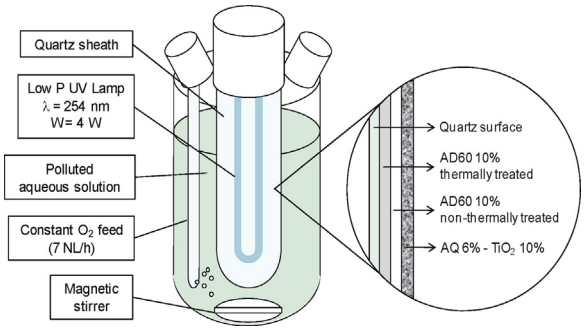

Fig. 2. Experimental apparatus and details of the photoactive coating.

hydrophilicity and consequently good wettability to the photoactive coating, while the backbone of the polymer is hydrophobic due to the presence of C—F bonds. AD is a random copolymer of TFE and 2,2,4-trifluoro-5-trifluoromethoxy-1,3-dioxole (TTD), characterized by outstanding chemical stability [24], low refractive index (equal to 1.327) and T_g of 130 °C [24]. AD was employed in solution during the experimental tests, using GALDEN® HT110 (Solvay Specialty Polymers) as solvent. GALDEN® HT110 is a PFPE-based solvent with boiling point of 110 °C and formula as follow: $CF_3O(CF_2CF(CF_3)O)_p(CF_2O)_nCF_3$ ($p+n=2$–3; $p/n=20$–50). Rhodamine B-base (RhB – Sigma–Aldrich® – dye content 97%) is an organic dye with formula $C_{28}H_{30}N_2O_3$ (MW = 442.55 g/mol; molecular structure in Fig. 1c) and water solubility of 11,000 mg/L. $BaSO_4$ micrometric powder (Laviosa Chimica Mineraria S.p.A. – Livorno) is insoluble in water and photochemically inert and it was chosen as white solid to generate turbidity in solution. The average particle size was estimated by SEM analysis and it was found to be in the range between 1 and 20 μm.

2.2. Photoactive coating

The deposition of an endurably stable photoactive coating on the quartz sheath (Fig. 2) was obtained by employing two different perfluoropolymer in solutions: a 10 wt% solution of AD (Fig. 1c) in Galden® HT110 perfluoropolyether [36] and a 6% solution of AQ (Fig. 1d) in a hydroalcoholic solvent (water/*i*-propanol/*n*-propanol 20:40:40) containing 10 wt% of dispersed active nanometric TiO_2. The former acted as hydrophobic fluorinated primer and the latter as photoactive layer (see preparation details in the Supporting information, S.I.).

The first two layers in contact with the UV source consisted in AD polymer. The first one was directly in contact with the quartz sheath surface and acted as hydrophobic primer coating. It was thermally cured (as described in the S.I.) in order to increase the adhesion between the coating and the quartz surface; moreover, this layer prevented water from penetrating between the coating and the sheath. This undesired phenomenon could cause rapid detachment of the photoactive coating from the quartz substrate and, consequently a severe loss of photocatalytic activity is observed. The second AD polymeric layer was not thermally treated and it allowed the adhesion between the perfluorinated hydrophobic layer and the ionomeric hydrophilic photoactive layer by a simple entanglement of the fluorinated chains.

The fine dispersion of TiO_2 (average aggregate dimension = 1 μm) in the hydroalcoholic AQ solution was performed by ultra-sonication for 30 min at room temperature in order to homogenize the catalyst into the ionomeric mixture before its application on the UV sheath. Due to its hydrophilicity, the AQ outer layer guaranteed significant pollutant permeability, promoting the direct contact between the activated TiO_2 and the pollutant RhB. Both polymeric AD and AQ layers in which the photocatalyst was embedded were chemically stable toward the degradation effects due to TiO_2 photocatalytic activity [20]. As P-25 photocatalyst can suffer rutilization process only at calcination temperatures, we assumed that the thermal curing of AQ polymeric layer (as described in the S.I.) did not affect both its phase and band gap [37].

2.3. Experimental apparatus

The reaction apparatus (Fig. 2) consisted of a stirred semi-batch 0.5 L glass reactor (diameter = 6.5 cm), realized to contain a low pressure Hg UV lamp (Engelhard Hanovia®, with nominal power absorption of 4 W, emitting light at wavelengths of 240–300 nm with emissivity of 0.2 W/m^2), inserted into a 2 mm thick quartz sheath. The UV lamp was cooled with a flux of nitrogen in order to maintain constant the solution temperature ($T = 25 \pm 3$ °C).

The emissivity of the UV lamp was measured with a Delta Ohm HD 2102.2 radiometer in the presence of the coated as well as uncoated quartz sheath. Due to the lamp geometry, the emissivity resulted constant along its cylindrical bulb and significantly decreased at the tip. The photoactive coating caused an evident variation in the lamp emissivity values. In fact, the average light intensities from the sheath surface were $(123 \pm 7) \times 10^{-3}$ W/m^2 for the uncoated quartz sheath and $(57 \pm 4) \times 10^{-3}$ W/m^2 after the application of the photoactive coating. The observed decrease in emissivity was higher than about 54% and it was completely ascribable to the UV absorption by TiO_2, because of AQ and AD UV transparency.

Overall, the AQ-based photocatalytic coating resulted adherent to the external surface of the sheath and in direct contact with the aqueous polluted solutions, with a surface/volume ratio of 0.048 m^2/L. The specific catalyst amount was found to be 0.120 g/m^2. The average thickness of the photoactive coating was measured by a UBM Microfocus laser profilometer and it was found equal to 5.80 ± 0.43 μm. The average photon flux (Φ) guaranteed by the employed low pressure Hg UV lamp was found equal to 15.71×10^{16} photons/(m^2 s); in the presence of the photoactive coating, the fraction of photon flux absorbed by dispersed TiO_2 was 8.43×10^{16} photons/(m^2 s), while the remaining radiation reached the polluted aqueous solution (see details in the S.I.). The average light intensity outside the reactor in the presence of dispersed TiO_2 powder particles (slurry) was $(68 \pm 3) \times 10^{-3}$ W/m^2 and, therefore, the fraction of photon flux absorbed by the catalyst slurry resulted 8.69×10^{16} photons/(m^2 s), considering negligible the absorption due to RhB (about 2×10^{-3} W/m^2). Oxygen is required in the photocatalytic reaction and it was fed at the bottom of the reactor. The oxygen flux was regulated at 7 NL/h in the presence of constant magnetic stirring: these two actions generated enough turbulence into the system to assume a constant concentration of O_2 in solution and into the photoactive coating, along with a homogeneous concentration of RhB.

2.4. Experimental procedure

The photocatalytic activity of the TiO_2-embedded perfluorinated coating was evaluated by monitoring the RhB abatement trends. These were obtained by, considering at different times, the percentage variation of the dye concentration in solution, as measured on the basis of its absorbance peak at 554 nm by the Lambert–Beer law (see further detailed description of the experimental procedure in the S.I.). RhB abatement was evaluated in the presence of the photoactive coating (**Pc-C** test) under UV irradiation. The photoactivity of the TiO_2-embedded coating was also measured in turbid conditions (**Pc-Ct** test), obtained by adding $BaSO_4$ microparticles (8 g/L, average particle dimension = 10 μm) to the RhB solution. The absorption of RhB on $BaSO_4$ particles resulted

Table 1
Experimental conditions of kinetic tests.[a]

Test	Description[b]	Catalyst	UV lamp emissivity (W/m^2)	TiO_2 slurry (mg/L)	$BaSO_4$ (g/L)
Pc-C	Photocatalysis	Photoactive coating[b]	0.2	0	0
Pc-Ct	Photocatalysis in turbid conditions[c]	Photoactive coating[b]	0.2	0	8[c]
Pc-S	Photocatalysis in slurry	TiO_2 powder	0.2	8	0
Pc-St	Photocatalysis in slurry and turbid conditions[c]	TiO_2 powder	0.2	8	8[c]
Ph-C	Photolysis(*Barrier coating*)[d]	–	0.2	0	0
Ph-t	Photolysis in turbid conditions[c]	–	0.2	0	8[c]
Abs-C	Absorption	Photoactive coating[b]	0	0	0
Abs-S	Absorption in slurry	TiO_2 powder	0	8	0

[a] $[RhB]_0 = 8 \times 10^{-6}$ M; $T = 25 \pm 3$ °C; constant stirring; and O_2 feed = 7 NL/h.
[b] See details in the S.I.
[c] Turbid conditions were obtained by dispersing $BaSO_4$ powder in the aqueous RhB solution.
[d] Barrier coating is a photoactive coating deactivated with two additional AD layers.

negligible, as evaluated by the decrease in RhB concentration in an aqueous RhB/$BaSO_4$ dispersion stirred for 24 h (see details in the S.I.). The photocatalytic coating activity was compared with the performances obtained by a suspension of TiO_2 powder (slurry), both in standard (**Pc-S** test) and in an increased turbidity conditions, obtained by adding $BaSO_4$ particles (**Pc-St** test) (see details in the S.I.). Since the dye removal in the **Pc-C** photocatalytic test was due to simultaneous different phenomena, e.g., photocatalysis, direct UV-promoted photolysis and absorption into the photoactive coating, appropriate accessory tests were performed in order to evaluate each contribution to RhB degradation, as reported in Table 1.

The **Ph-C** test was a photolysis experiment realized under UV irradiation by depositing on the active coating two additional UV transparent AD layers (barrier coating) which prevented the RhB diffusion from the solution into the ionomeric photocatalytic layer (see details in the S.I.); **Abs-C** was an absorption test run in the presence of the photoactive coating and in the absence of UV irradiation. RhB removal due to photolysis in the presence of $BaSO_4$ (**Ph-t** test) and RhB absorption on TiO_2 powder (**Abs-S** test) were also evaluated. Each TiO_2 slurry test (**Pc-S**, **Pc-St**, and **Abs-S)** was performed by dispersing the same amount of TiO_2 photocatalyst (8 mg/L) which was contained in the photoactive coating used in the tests **Pc-C**, **Pc-Ct**, **Ph-C** and **Abs-C**. In the presence of this amount of TiO_2, dark zones inside the reactor due to catalyst slurry were negligible; indeed the catalyst performances revealed a decrease in the photocatalyst efficiency only when the TiO_2 content was higher than 0.66 g/L [3]. The photoabatement was also qualitatively monitored by observing the hue variations of the photoactive coating during the tests.

2.5. Fluorine-19 nuclear magnetic resonance (^{19}F NMR) spectroscopy

^{19}F NMR experiments were performed on a Bruker 500 Ultrashield spectrometer operating at 470.30 MHz. In particular, samples of the solution collected from the reactor at the end of the photoabatement tests were analyzed by ^{19}F NMR, using D_2O as a deuterated solvent. The absence of signals ascribable to any water-soluble fluorine-containing compounds in the aqueous solution can

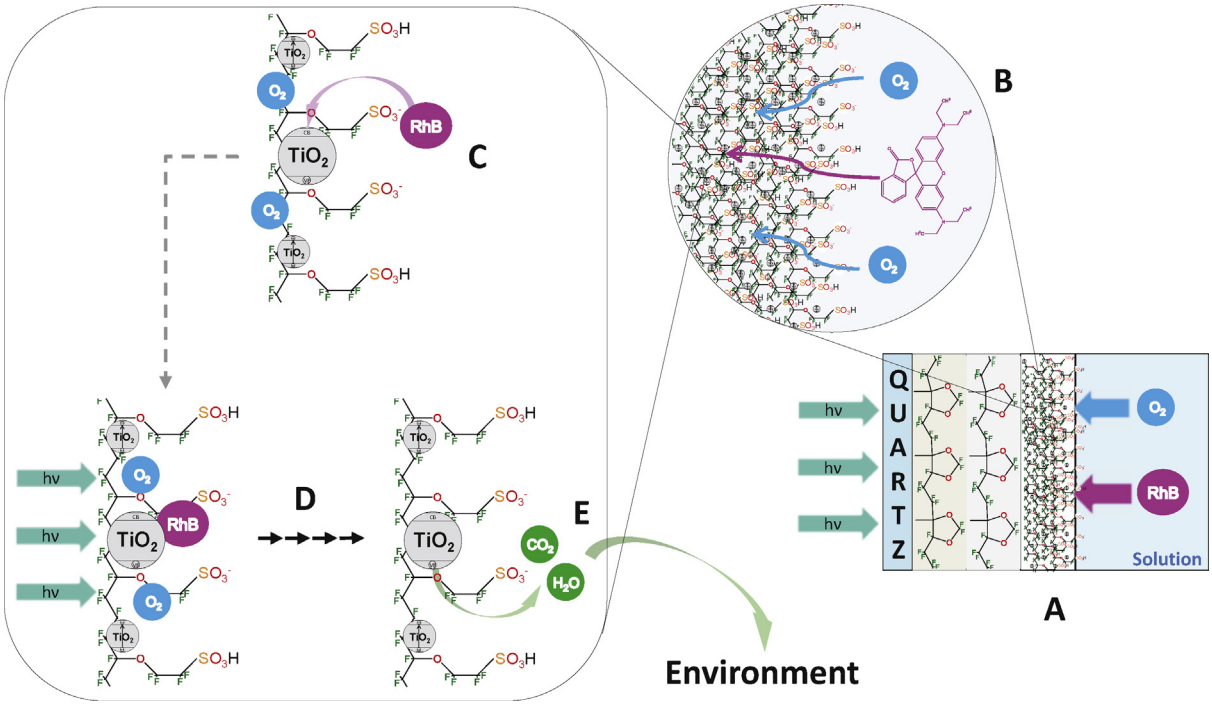

Fig. 3. Photocatalytic coating operating mode: migration of RhB and O_2 molecules toward the aqueous solution-polymer interface (A); RhB and O_2 phase-transfer and diffusion into the ionomeric phase (B); RhB and oxygen adsorption on TiO_2 particles (C); stepwise RhB degradation (oxidation) by photoactivated TiO_2 particles (D); and retro-diffusion of mineralized products in the aqueous phase (E).

confirm the chemical stability of the polymeric layers (AQ and AD) in the perfluorinated photoactive coating.

2.6. MS/MS analysis

MS/MS analyses were performed in order to verify the presence of RhB degradation intermediates in the aqueous solution during the photocatalytic kinetic tests. MS/MS analyses were done with a Bruker Esquire 3000 Plus quadrupole ion trap mass spectrometer (Bruker Daltonics) operating in positive electrospray mode. The aqueous samples were diluted with acetonitrile (volume ratio 1:3) before being injected.

3. Results and discussion

Perfluorinated ionomers exhibit high ion-exchange capacities in water, in these conditions hydrophilic continuous water phases inside the hydrophobic fluorinated matrix are formed [27,38]. This multi-phase matrix is characterized by strongly acid sulfonic moieties and it is responsible for the superior ion conductivity typical of the fluorinated membranes.

The strong hydrophilicity of the ionomeric matrix promoted synergic interactions between the TiO_2-containing photoactive coating and the aqueous polluted solution. RhB molecules were homogeneously dispersed in the aqueous solution and they could reach the aqueous solution-polymer interface due to simple convection and diffusion (Fig. 3A). The presence of the acidic sulfonic side chain terminals promoted the RhB phase-transfer from the aqueous solution-polymer interface into the water phases within the ionomeric matrix (Fig. 3B). Thus, the acidic nature of the ionomeric photoactive layer promoted an increase in the RhB concentration localized in the immediate vicinity of the immobilized TiO_2 particles. Molecular oxygen penetrated into the photoactive coating due to the high permeability of AQ and AD polymers toward this gas (Fig. 3B). In the AQ ionomer the organic pollutant molecules reached the embedded photocatalyst TiO_2 particles by diffusion and were adsorbed on them (Fig. 3C); in the presence of UV light and oxygen, RhB was degraded by photoactivated TiO_2 particles (Fig. 3D), generating mineralization products which retro-diffused to the aqueous phase (Fig. 3E). A comparison of the kinetic curves obtained from the main photocatalytic tests is shown in Fig. 4.

The photoactive coating (**Pc-C** and **Pc-Ct** tests) evidently guaranteed higher RhB abatement rates than TiO_2 powder as a slurry (**Pc-S** test). This surprising result appeared to be in agreement with a synergic effect between the acid/base reactions promoted by the ionomeric superacidic material and the photodegradation properties of TiO_2 photocatalyst. The synergism is particularly evident at very low pollutant concentration where the photoactive coating is very active if compared to the standard TiO_2 slurry (see Fig. 4 and Fig. 5A).

Moreover, it was reasonable to assume that during the photocatalytic tests RhB diffused into the photocatalytic layer and was promptly degraded by the light-induced abatement reactions. Therefore, its content in the photocatalytic layer and on the active TiO_2 was considered negligible. On the contrary, the chemical stability of both AD and AQ was confirmed by ^{19}F-NMR analysis which revealed the absence of signals ascribable to fluoride release in the aqueous solution during RhB photoabatement.

Degradation reactions appeared to follow pseudo-first order kinetics (correlation coefficient $R^2 > 0.99$ – Fig. 5) which enabled the comparison of the apparent rate constants (k_{app}).

The comparison between the linearized kinetic curves of RhB photodegradation reactions obtained during **Pc-C** and **Pc-S** tests as well as **Pc-Ct** and **Pc-St** tests is reported in Fig. 5A and B, respectively. Linearized kinetic curves of RhB absorption by **Abs-C** and **Abs-S** tests as well as RhB photolysis by **Ph-t** and **Ph-C** tests are compared in Fig. 5C and D.

The photoactive coating guaranteed a photoabatement rate with a $k_{appPc\text{-}C}$ of 0.0923 min^{-1}: this value is more than three times higher than $k_{appPc\text{-}S}$ obtained in **Pc-S** test (Fig. 5A). During the **Pc-C** test, a RhB degradation of 76% was reached in 15 min and the pollutant was completely removed after 60 min, as reported in Table 2 (see Table S.I. 1 for the full degradation data). The TiO_2-embedded photoactive coating resulted photocatalytically more active than dispersed titanium dioxide, even at low RhB concentration. Indeed, the **Pc-S** test with TiO_2 slurry as a catalytic system revealed a RhB degradation of 78% after 60 min, corresponding to a photoabatement rate, $k_{appPc\text{-}S}$, of 0.0250 min^{-1}; moreover, in this test, the complete degradation of RhB was obtained after 180 min (see S.I. Table 1).

The photocatalytic activity of the TiO_2-embedded photoactive coating was partially affected by the presence of $BaSO_4$ particles (8 g/L). In the **Pc-Ct** test (Fig. 5-B), an abatement of RhB equal to 95% was reached after 60 min (see Table 2) and the photoabatement rate, $k_{appPc\text{-}Ct}$, resulted 0.0546 min^{-1}. This value is lower than

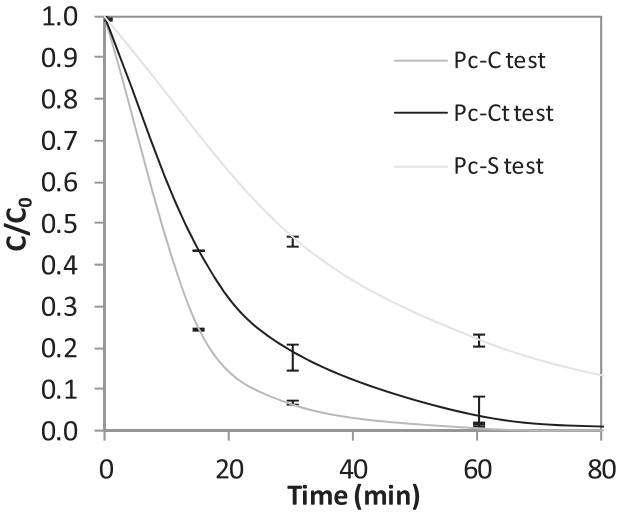

Fig. 4. RhB photodegradation kinetic curves obtained by using the photoactive coating (**Pc-C** test), the photoactive coating in turbid conditions (**Pc-Ct** test) and TiO_2 slurry (**Pc-S** test).

Table 2
Calculated apparent kinetic constants and percent degradation after 60 min treatment.

Test	Description (catalyst)	k_{app} (min^{-1})	deg$_{60}$ (%)
Pc-C	Photocatalysis (photoactive coating)	0.0923	99.1
Pc-Ct	Photocatalysis in turbid conditions[a] (photoactive coating)	0.0546	95.0
Pc-S	Photocatalysis in slurry (TiO_2 powder)	0.0250	77.9
Pc-St	Photocatalysis in slurry and turbid conditions[a] (TiO_2 powder)	0.0085	41.9
Ph-C	Photolysis (barrier coating on photoactive coating)	0.0076	34.8
Ph-t	Photolysis in turbid conditions[a]	0.0040	24.7
Abs-C	Absorption (photoactive coating)	0.0271	78.1
Abs-S	Absorption in slurry (TiO_2 powder)	0.0035	16.8

[a] Turbid conditions were obtained by dispersing $BaSO_4$ powder (8 g/L) in the aqueous RhB solution.

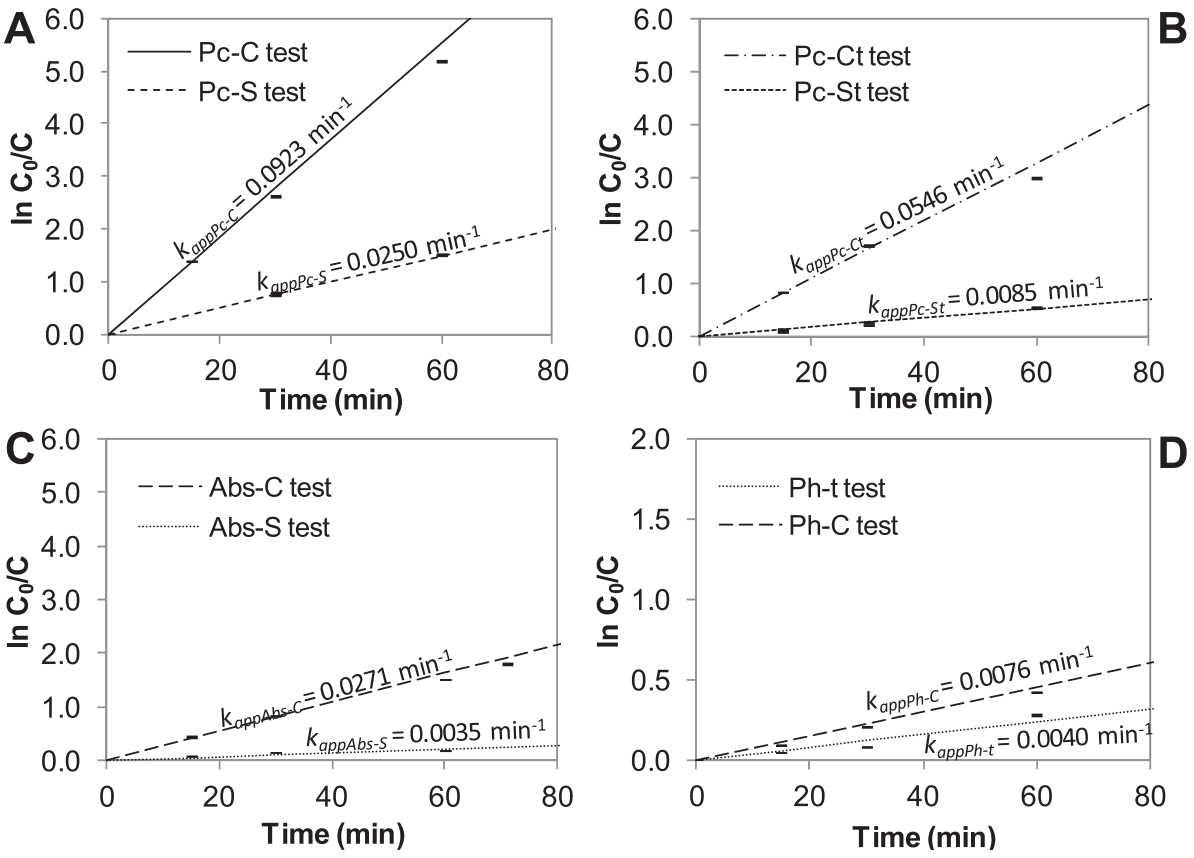

Fig. 5. Linearized kinetic curves with apparent kinetic constant values (k_{app}) of RhB removal. Kinetic comparison between: photocatalysis using the photoactive coating (**Pc-C** test) and TiO_2 slurry (**Pc-S** test) (A); photocatalysis in the presence of $BaSO_4$ particles using the photoactive coating (**Pc-Ct** test) and TiO_2 slurry (**Pc-St** test) (B); absorption on the photoactive coating (**Abs-C** test) and on TiO_2 slurry (**Abs-S** test) (C); and photolysis in the presence of $BaSO_4$ particles (**Ph-t** test); photolysis with the photoactive coating in the presence of the barrier coating (**Ph-C** test) (D).

$k_{appPc-C}$ and this result could be attributed to the strongly diminished photolysis contribution to RhB degradation due to the highly turbid conditions of **Pc-Ct** test due to dispersed $BaSO_4$ particles (8 mg/L) (see Table 1). The transparent-white hue of the photocatalytic coating at the end of the photoactive coating tests (**Pc-C** and **Pc-Ct**) revealed that the absorbed RhB was completely decomposed during the photocatalytic oxidation. The UV blocking effect due to turbidity was more evident in **Ph-t** and **Pc-St** tests in which $BaSO_4$ particles (8 mg/L) were dispersed. In both cases the RhB removal rate ($k_{appPh-t}$ and $k_{appPc-St}$) was very low, reaching values equal to 0.0040 min^{-1} and 0.0085 min^{-1}, respectively (see Table 2 and Fig. 5B and D).

The overall process of RhB abatement was due to different phenomena, such as photocatalysis, UV-promoted photolysis and absorption of the pollutant into the photoactive coating or onto TiO_2 slurry particles. Therefore, the apparent kinetic constants which described the disappearance of RhB from the solutions ensued from these different contributions. Both absorption tests (**Abs-C** and **Abs-S**) and photolysis tests (**Ph-C** and **Ph-t**) were also performed and compared (Fig. 5C and D). In the **Abs-C** test, the RhB dye was chemically stable during the migration from the solution into the photoactive coating and at the end of the test the photoactive coating appeared colored with the typical bright pink hue of RhB. The decrease in RhB concentration observed during absorption tests could be described as a simple mass transfer of the pollutant from the aqueous phase to the photocatalytic coating (**Abs-C**) or onto TiO_2 slurry particles (**Abs-S**).

The photolysis test in the presence of the barrier coating (**Ph-C**) was specifically set in order to avoid RhB absorption into the ionomeric coating, maintain the UV absorption due to the presence of the photoactive coating and highlight only the RhB photolysis due to UV light that passed through the photoactive coating (Fig. 5D). This effect was obtained by depositing on the active coating two additional UV transparent AD layers which acted as barrier coatings to RhB (Tables 1 and 2, and S.I. for details). In addition, the comparison of the calculated kinetic parameters presented in Table 2 allowed to assess that the dye absorption onto the catalyst slurry particles ($k_{app\ Abs-S}$ = 0.0035 min^{-1}) resulted negligible if compared to the corresponding photodegradation rate ($k_{appPc-S}$ = 0.0250 min^{-1}).

RhB photoabatement was also monitored by MS/MS analysis in order to verify the presence of RhB degradation intermediates. In **Pc-C** and **Pc-Ct** test, the signals in the mass spectra of water phase were ascribable only to the presence of RhB (*m*/*z*: 443 $[M+H]^+$, 413, 399, 307, and 143) and no evidences of other organic compounds due to RhB partial degradation were observed. Hence, the photoactive coating mineralized the organic dye without retro-diffusion of partial degradation intermediates to the aqueous solution. As expected, in the **Pc-S** (slurry) test several RhB partial degradation products were identified by MS analysis; in particular, MS signals related to *N*-deethylated intermediates, such as *N*-ethyl-*N*′-ethyl-rhodamine (*m*/*z*: 387 $[M+H]^+$), *N*-ethyl-rhodamine (*m*/*z*: 381 $[M+Na]^+$), rhodamine (*m*/*z*: 353 $[M+Na]^+$, 331 $[M+H]^+$), *N*-deethylated/carboxylated species (*m*/*z*: 279 $[M+Na]^+$), as well as lower molecular weight compounds were detected. Therefore, in the slurry system retro-diffusion of intermediates was observed, accordingly to literature [39,40].

Quantum yield (QY) and quantum efficiency (QE) of the abatement process were estimated through Eqs. (3) and (4) [41,42]:

$$QY = \frac{k_{aap}[RhB]_0 V}{\Phi_{Abs}} \quad (3)$$

$$QE = \frac{k_{app}[RhB]_0 V}{\Phi_{IN}} \quad (4)$$

where k_{app} is the calculated apparent kinetic constant expressed in s^{-1}, $[RhB]_0$ the initial concentration of RhB, V the volume of the solution, Φ_{Abs} the absorbed fraction of molar photon flux expressed in mol s^{-1} and Φ_{IN} the average molar photon flux guaranteed by the UV lamp. QY and QE were estimated for the photoactive coating (**Pc-C** test) and compared to the performances obtained with TiO_2 slurry (**Pc-S** test): in the **Pc-C** test, QY and QE were 92% and 49%, respectively; in the **Pc-S** test they resulted 23% and 13%, respectively. In particular, the light absorption due to the TiO_2 within the photoactive coating (66×10^{-3} W/m^2) resulted similar to that due to the TiO_2 slurry (55×10^{-3} W/m^2). Thus, the comparison of QY and QE values showed definitely higher yield and efficiency of the photoactive coating compared to the TiO_2 slurry. On the basis of these results, a further optimization of the performances of photoactive coating can be fruitfully obtained by increasing its thickness.

4. Conclusions

The TiO_2-embedded ionomeric perfluorinated coating is more than three times more efficient compared to TiO_2 in slurry conditions. This result was observed for polluted water solution both in clear as well as in turbid conditions, pointing out useful synergic effects between the ionomeric phase and the photoactive oxide. Immobilized TiO_2 particles, in fact, were not deactivated by slime interposition between the UV source and the photoactive coating and avoided onerous separation of the catalyst from the purified water. The characteristics of this photocatalytic system make it suitable for industrial employment for both sequential batch and continuous water management. Studies on visible light activated TiO_2, gas phase photo-induced pollutants depletion as well as kinetic modeling for process engineering are foreseeable and valuable research for this promising photoactive coating.

Acknowledgments

The authors wish to acknowledge with thanks the generous support and the valuable interactions induced to this research in the field of fluorinated materials by the institution of the Politecnico di Milano/Solvay Fluorine Chemistry Chair. This work has been supported by MIUR (PRIN 2010–2011).

Appendix A. Supplementary data

Supplementary data associated with this article can be found, in the online version, at http://dx.doi.org/10.1016/j.apcatb.2015.01.033.

References

[1] C. Galindo, P. Jacques, A. Kalt, Chemosphere 45 (2001) 997–1005.
[2] G. Mele, G. Ciccarella, G. Vasapollo, E. Garcia-Lopez, L. Palmisano, M. Schiavello, Appl. Catal. B 38 (2002) 309–319.
[3] M. Sansotera, F. Persico, C. Pirola, W. Navarrini, A. Di Michele, C.L. Bianchi, Appl. Catal. B 148 (2014) 29–35.
[4] A. Polo, M.V. Diamanti, T. Bjarnsholt, N. Høiby, F. Villa, M.P. Pedeferri, F. Cappitelli, Photochem. Photobiol. 87 (2011) 1387–1394.
[5] A. Fujishima, T.N. Rao, D.A. Tryk, J. Photochem. Photobiol. C 1 (2000) 1–21.
[6] K. Sato, T. Hirakawa, A. Komano, S. Kishi, C.K. Nishimoto, N. Mera, M. Kugishima, T. Sanoa, H. Ichinose, N. Negishi, Y. Seto, K. Takeuchi, Appl. Catal. B 106 (2011) 316–322.
[7] S.R. Seagle, in: J.I. Kroschwitz (Ed.), The Kirk Othmer Encyclopedia of Chemical Technology, vol. 24, 4th ed., John Wiley and Sons, New York, 1997, pp. 186–224.
[8] N.P. Mellott, C. Durucan, C.G. Pantano, M. Guglielmi, Thin Solid Films 502 (2006) 112–120.
[9] P. Pichat, in: E. Pelizzetti, N. Serpone (Eds.), Homogeneous and Heterogeneous Photocatalysis, NATO ASI Series, vol. 174, Springer, New York/Heidelberg, 1986, pp. 533–554.
[10] X.F. Li, K.L. Lv, K.J. Deng, J.F. Tang, R. Su, J. Sun, L.Q. Chen, Mater. Sci. Eng. B 158 (2009) 40–47.
[11] H. Park, W. Choi, J. Phys. Chem. B 108 (2004) 4086–4093.
[12] M.A. Henderson, Surf. Sci. Rep. 66 (2011) 185–297.
[13] J. Sun, X. Yan, K. Lv, S. Sun, K. Deng, D. Du, J. Mol. Catal. A: Chem. 367 (2013) 31–37.
[14] F. Persico, M. Sansotera, M.V. Diamanti, L. Magagnin, F. Venturini, W. Navarrini, Thin Solid Films 545 (2013) 210–216.
[15] A. Mills, S. Le Hunte, J. Photochem. Photobiol. A 108 (1997) 1–35.
[16] M.F.J. Dijkstra, A. Michorius, H. Buwalda, H.J. Panneman, J.G.M. Winkelman, A.A.C.M. Beenackers, Catal. Today 66 (2001) 487–494.
[17] J. Yu, L. Shi, J. Mol. Catal. A: Chem. 326 (2010) 8–14.
[18] T. Ohno, K. Sarukawa, K. Tokieda, M. Matsumura, Appl. Catal. B 17 (1998) 25–36.
[19] C.L. Bianchi, S. Ardizzone, G. Cappelletti, G. Cerrato, W. Navarrini, M. Sansotera, J. Mater. Res. 25 (2010) 96–103.
[20] W. Navarrini, T. Brivio, D. Capobianco, M.V. Diamanti, M.P. Pedeferri, L. Magagnin, G. Resnati, J. Coat. Technol. Res. 8 (2011) 153–160.
[21] D.M. Lemal, J. Org. Chem. 69 (2004) 1–11.
[22] C. Corvaja, G. Farnia, G. Formenton, W. Navarrini, G. Sandonà, V. Tortelli, J. Phys. Chem. 98 (1994) 2307–2313.
[23] M. Yamabe, H. Miyake, Organofluorine Chemistry, in: R.E. Banks, B.E. Smart, J.C. Tatlow (Eds.), Plenum Press, New York/London, 1994, pp. 397–410.
[24] W. Navarrini, M.V. Diamanti, M. Sansotera, F. Persico, M. Wu, L. Magagnin, S. Radice, Prog. Org. Coat. 74 (2012) 794–800.
[25] M. Avataneo, W. Navarrini, U. De Patto, G. Marchionni, J. Fluorine Chem. 130 (2009) 933–937.
[26] H. Zhang, P.K. Shen, Chem. Rev. (Washington, DC U. S.) 112 (2012) 2780–2832.
[27] W.G. Grot, Fluorinated ionomers, in: W. Andrew (Ed.), PDL Handbook Series, Elsevier, Amsterdam, 2008, pp. 75–135.
[28] J.R. O'Dea, N.J. Economou, S.K. Buratto, Macromolecules 46 (2013) 2267–2274.
[29] P. Wight, The Kirk Othmer Encyclopedia of Chemical Technology, in: J.I. Kroschwitz (Ed.), John Wiley and Sons, New York, 2000.
[30] Environment Canada, Health Canada, Screening Assessment for the Challenge: spiro [isobenzofuran-1(3H), 9'-[9H]xanthen]-3-one,3',6'-bis(diethylamino) (Solvent Red 49), www.ec.gc.ca/ese-ees/default.asp?lang=En&n=71ECF6F2-1, September 2010.
[31] T. Wu, G. Liu, J. Zhao, J. Phys. Chem. B 102 (1998) 5845–5851.
[32] Z. He, C. Sun, S. Yang, Y. Ding, H. He, Z. Wang, J. Hazard. Mater. 162 (2009) 1477–1486.
[33] T.S. Natarajan, M. Thomas, K. Natarajan, H.C. Bajaj, R.J. Tayade, Chem. Eng. J. 169 (2011) 126–134.
[34] S. Tawkaew, S. Yin, T. Sato, Int. J. Inorg. Mater. 3 (2001) 855–859.
[35] J. Aguado, R. van Grieken, M.J. López-Muñoz, J. Marugán, Appl. Catal. A 312 (2006) 202–212.
[36] A. Russo, W. Navarrini, J. Fluorine Chem. 125 (2004) 73–78.
[37] G. Colón, M.C. Hidalgo, J.A. Navio, Appl. Catal. A 231 (2002) 185–199.
[38] W. Navarrini, B. Scrosati, S. Panero, A. Ghielmi, A. Sanguineti, G. Geniram, J. Power Sources 178 (2008) 783–788.
[39] Y.M. Xu, C.H. Langford, J. Photochem. Photobiol. A 133 (2000) 67–71.
[40] Y. Li, S. Sun, M. Ma, Y. Ouyang, W. Yan, Chem. Eng. J. 142 (2008) 147–155.
[41] N. Serpone, J. Photochem. Photobiol. A 104 (1997) 1–12.
[42] D. Gerster, J. Reichert, H. Bi, J.V. Barth, S.M. Kaniber, A.W. Holleitner, I. Visoly-Fisher, S. Sergani, I. Carmeli, Nat. Nanotechnol. 7 (2012) 673–676.